Static magnetic properties and relaxation of the ternary mixed magnetic insulating system $Co_{1-x}Mn_yFe_{x-y}Cl_2 \cdot 2H_2O$

G. C. DeFotis, C. D. Wallo, R. L. Smith, D. B. Bodkin, G. L. Mirabilio, T. R. Leftwich, M. G. Kim, and Z. D. Reed

Chemistry Department, College of William and Mary, Williamsburg, Virginia 23187-8795, USA

The properties of mixed ternary magnetic $Co_{1-x}Mn_yFe_{x-y}Cl_2 \cdot 2H_2O$ are examined by dc magnetization and susceptibility measurements, from 1.8 to 300 K, for twelve mixtures reasonably spanning composition space. The possible binary mixtures were studied previously; that with Fe and Co components has competing orthogonal anisotropies, that with Co and Mn components competing ferromagnetic and antiferromagnetic exchange interactions, and that with Fe and Mn components both sources of competition. For ternary compositions the Curie and Weiss constants, in $\chi_M = C/(T-\theta)$ fits to high temperature susceptibilities, are fairly well (C) and less well (θ) accounted for as weighted averages of pure component values. Maxima and/or other anomalies in low temperature susceptibilities are used to construct a $T(x,y)$ magnetic phase diagram. Magnetization vs field isotherms exhibit different shapes as a function of composition. Magnetic irreversibility, from field cooled vs zero-field cooled magnetization data, varies markedly with composition. For one mixture the temperature-field irreversibility line is determined; it conforms to an unusual intermediate anisotropy case. The thermoremanent magnetization (TRM) decays as $\ln(t)$, and shows an $\exp(-\beta T)$ temperature dependence. $T \log_{10}(t/\tau_0)$ scaling of the TRM is also found, with $\tau_0 = 10^{-12}$ to 10^{-13} s. These spin glass characteristics presumably arise from randomness and competing ferromagnetic and antiferromagnetic exchange interactions. Magnetic irreversibility is promoted by a majority Co plus Mn content, with Mn at least somewhat more prevalent than Co.

I. INTRODUCTION

The vast majority of studies of randomly mixed magnetic systems have been concerned with binary (two-component) mixtures. Even apart from their relative theoretical simplicity (though the variety of predicted behavior is still remarkably rich), binary mixtures can be realized from among a large number of chemical and structural families of materials. It is usually possible to find at least two members of such a family which will mix homogeneously. One such family, and a fairly simple one structurally, is $MCl_2 \cdot 2H_2O$. The manganese, iron and cobalt members are isostructural, with only fairly modest differences in lattice parameters.[1,2] Chemical and structural $MCl_2MCl_2M\ldots$chains characterize the materials, along which exchange interactions may be ferromagnetic (Fe and Co) or antiferromagnetic (Mn), with the chains fairly strongly coupled both structurally and magnetically (with antiferromagnetic interactions).

The first binary mixture prepared from the above family, and one of the most important binary mixed magnets to be studied, was $Fe_{1-x}Co_xCl_2 \cdot 2H_2O$.[3–6] Competing orthogonal anisotropies occur in this case, and the data implied the existence of a tetracritical point, consistent with a general theoretical prediction.[7] A second mixture from the same family, $Fe_{1-x}Mn_xCl_2 \cdot 2H_2O$, was then studied.[8–10] This is a more complicated case than in the Fe/Co mixture because both competing orthogonal anisotropies and competing ferromagnetic and antiferromagnetic exchange interactions occur. Theoretical attention had also been directed to situations exhibiting this second type of competition between different sign exchange interactions.[11] In the Fe/Mn mixture an apparent tetracritical point, oblique antiferromagnetic ordered

phase, and spin glass phases were observed, in keeping with theoretical expectations. The remaining binary mixture based on the three indicated components, $Co_{1-x}Mn_xCl_2 \cdot 2H_2O$, was then studied and found to be characterized by an exceptionally different $T-x$ magnetic phase diagram,[12–14] including spin glass regions arising from the competition between ferromagnetic and antiferromagnetic interactions combined with disorder. Much attention was also devoted to this mixture by other experimental methods.[15–18]

Despite the greater complexity of a three component magnetic mixture, such a system should be worth examination. It is more difficult to identify chemical families from which three members can be successfully admixed, and which also offers some motivation for doing so. But one such is just the $MCl_2 \cdot 2H_2O$ series described above. Each of the three components (Mn, Fe and Co) differs from the others in terms of exchange interaction distribution or crystalline anisotropy characteristics or both. Each of three possible binary mixtures has been well studied. The absence of any indications of inhomogeneity in previous work on three different binary combinations leads one to expect no problems concerning ternary mixtures. Because of the contrasting behaviors in the three binary mixtures, including the form of their temperature-composition magnetic phase diagrams, the ternary mixture $Co_{1-x}Mn_yFe_{x-y}Cl_2 \cdot 2H_2O$ is very worth investigating. A comparative crystallographic and spin structure diagram appears in Ref. 25.

Ternary magnetic mixtures are not unknown, especially among metallic systems, but have hardly been investigated from a broad ranging composition variation perspective. They are also much less well represented among insulating systems. Thus, the metallic alloys Fe-Ni-Cr, Fe-Ni-Mn,

and Cr-Fe-Mn have been studied,[19–21] but only over very limited composition ranges; some theoretical work has also been devoted to the second of these systems.[22] In the present context comparison with insulating materials is preferable in principle. But except for certain Prussian blue type systems, where three or even four magnetic ions occur, but where rather limited composition ranges only have been explored and where the focus was not on magnetic phase diagram or global magnetic behavior issues,[23,24] ternary insulators are unexplored.

In this paper we present data and analysis for twelve different compositions of $Co_{1-x}Mn_yFe_{x-y}Cl_2 \cdot 2H_2O$, planned and prepared in order to reasonably span the two-dimensional composition space of a ternary system. Partial results for six of the compositions have been presented;[25,26] previously displayed data are not repeated here. Static magnetization and susceptibility measurements as a function of temperature, field and time are employed. The temperature-composition phase diagram and dependence of various properties including irreversibility on composition are major points of interest.

II. EXPERIMENT

Reagent grade $CoCl_2 \cdot 6H_2O$ and $MnCl_2 \cdot 4H_2O$ were dissolved in water in the desired molar proportions, then purged of dissolved oxygen by extensive bubbling with inert gas. Carefully measured quantities of newly made and standardized aqueous $FeCl_2$ solution, prepared in such a way as to eliminate Fe^{3+} impurities and dissolved oxygen, was then added. The resulting ternary solutions were purged again, then placed in a vacuum oven which was flushed with Ar(g), and held at 80 °C for several days until reaching dryness. The polycrystalline solid materials obtained were confirmed to be dihydrate by thermogravimetric analysis. X-ray diffraction patterns suggested that the mixtures were microscopically homogeneous at the level probed by this technique. Compositions reported in the following are nominal. Previous work on the Fe/Mn and Co/Mn binary mixtures showed that actual compositions of samples measured magnetically differed insignificantly (0.005 mole fraction unit or less) from nominal, and that any concentration gradients for a given preparation were at a similar low level.

A variable temperature vibrating sample magnetometer system was used to make magnetization and susceptibility measurements. Except where indicated, data presented in the following are field-cooled measurements, with corrections (rather small) applied for demagnetization and diamagnetism. Polycrystalline samples of approximately 100 mg size were quickly packed under dry conditions into nonmagnetic sample holders, weighed, and then screwed onto a nonmagnetic sample rod in immediate proximity to a calibrated carbon-glass resistance thermometer. Temperatures are estimated to be accurate to ±0.005–0.5 K, depending on the range, magnetic field values to ±max(2G, 0.1%), and magnetization and susceptibility data to 1.5% absolute, with a precision much better than this. For zero-field-cooling experiments, a small external power supply was used to cancel the residual field of the electromagnet.
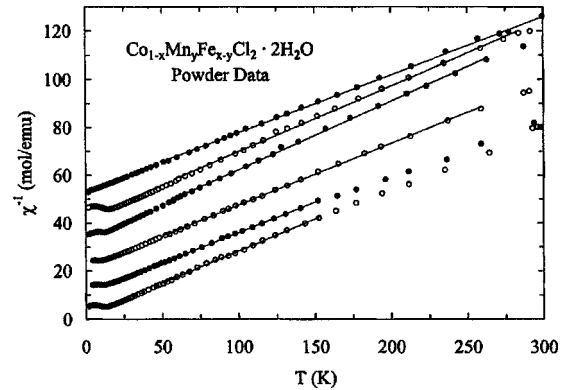

FIG. 1. Inverse molar magnetic susceptibility vs temperature for various compositions of $Co_{1-x}Mn_yFe_{x-y}Cl_2 \cdot 2H_2O$. From bottom to top the compositions and the shifts in mol/emu (for clarity) are $(1-x, y)$ shift = (0.320, 0.200) 0; (0.101, 0.494) 10; (0.231, 0.423) 20; (0.638, 0.112) 30; (0.333, 0.067) 40; (0.090, 0.810) 50. Lines are Curie-Weiss fits described in text.

III. MEASUREMENTS AND ANALYSIS

A. Magnetic susceptibility

The reciprocal molar susceptibilities of six compositions for which this property has not been displayed before appear in Fig. 1. Linear regimes generally extend from about 50 K to the highest temperatures measured, though sometimes instrumental instabilities lead to less reliable higher temperature data which are then not included in the Curie-Weiss fits according to $\chi_M = C/(T - \theta)$. In Table I appear the C and θ values obtained for the twelve compositions studied. Statistical uncertainties in the fitted parameters are typically of the order 0.01 emu K/mol in C and 0.4 K in θ. Also included in the table are calculated Curie and Weiss constants obtained assuming them to be mole-fraction weighted averages of corresponding values for the three pure components. For the latter we have employed results from our own measurements on $MnCl_2 \cdot 2H_2O$, $CoCl_2 \cdot 2H_2O$, and $FeCl_2 \cdot 2H_2O$ in a comparable temperature range as for the present mixed samples: $C = 4.46_0$, 3.03_5, and 3.53_2 emu K/mol and $\theta = -14.5$, -7.5, and 1.7_5 K for the Mn, Co, and Fe components, respectively. This should be preferable to employing literature or other values based on fits to relatively lower temperature data arguably outside a proper Curie-Weiss range. Hence some calculated values differ from those presented previously.[25,26] The weighted average assumption should be more reliable for the single-ion property C than for θ, which is a multi-ion interaction parameter. Further consideration of Table I is postponed to the Discussion section.

In Figs. 2 and 3 appear the molar magnetic susceptibilities of the same six compositions in the low temperature region; for the other six compositions in Table I $\chi(T)$ at low temperatures has appeared previously.[25,26] With one exception, each of the compositions in these figures exhibits a definite maximum; in the $Co_{0.090}Mn_{0.810}Fe_{0.100}Cl_2 \cdot 2H_2O$ mixture of Fig. 3 the maximum in merely incipient, but unmistakable nonetheless. The locations of the maxima span a substantial range in temperature, and are listed in Table II as T(max). Additional feature(s) appear at lower temperatures than that

TABLE I. $Co_{1-x}Mn_yFe_{x-y}Cl_2 \cdot 2H_2O$ compositions and Curie-Weiss fit parameters.

$1-x$	y	$x-y$	C(emu K/mol)	θ(K)	C_{calc}(emu K/mol)	θ_{calc}(K)
0.377	0.464	0.159	3.67	−8.1	3.79	−9.3
0.461	0.377	0.162	3.58	−9.5	3.65	−8.6
0.634	0.272	0.094	3.62	−14.2	3.47	−8.5
0.170	0.681	0.149	4.13	−10.0	4.08	−10.9
0.152	0.240	0.608	3.58	0.1	3.68	−3.6
0.320	0.200	0.480	3.74	−5.9	3.56	−4.5
0.101	0.494	0.405	3.93	−2.2	3.94	−7.2
0.231	0.423	0.346	3.87	−6.1	3.81	−7.3
0.638	0.112	0.250	3.49	−12.6	3.32	−6.0
0.333	0.067	0.600	3.66	−9.4	3.43	−2.4
0.090	0.810	0.100	4.12	−14.3	4.24	−12.2
0.535	0.170	0.295	3.47	−5.5	3.42	−6.0

of any prominent χ(max); the locations of these features, which may be associated with possible transitions, are also listed in Table II. The first such column gives an estimate of T_c associated with T(max), where it can be made. This is either where $d\chi/dT$ appears to be largest on the low temperature side of the maximum, the standard criterion, or where some other anomaly in this region is evident. The occurrence of susceptibility maxima at temperatures comparable to those characterizing the three pure components is more frequent among the eight compositions examined more recently; among the first four mixtures studied only one, $Co_{0.634}Mn_{0.272}Fe_{0.094}Cl_2 \cdot 2H_2O$, showed a clear maximum. Yet any obvious compositional systematics which might explain this difference is not evident. For example, to the extent that oxidation of Fe^{2+} to Fe^{3+} could explain the absence of susceptibility maxima (because of a strong Fe^{3+} paramagnetic impurity contribution), the first four mixtures listed in the tables (and the first studied) are least likely to be affected because of their low iron content.

B. Magnetization vs field isotherms

Magnetization vs field isotherms appear below for several of the compositions examined. These examples will display both representative aspects and most of the more interesting behavior appearing in $M(H)$ as a function of temperature. In each case, the sample was cooled to the target temperature in near zero field, after which the field was gradually increased to 15.9 kG and then decreased back down.

The isotherms of $Co_{0.152}Mn_{0.240}Fe_{0.608}Cl_2 \cdot 2H_2O$ in Fig. 4 are typical of several of the twelve compositions examined. There is virtual linearity of the 4.2 K isotherm, with negligible hysteresis, but some small convex downward curvature in the 2.6 K and 1.85 K isotherms, though also with negligible or at a rate very small hysteresis. Quite similar behavior occurred for the isotherms of $Co_{0.634}Mn_{0.272}Fe_{0.094}Cl_2 \cdot 2H_2O$. The isotherms of $Co_{0.377}Mn_{0.464}Fe_{0.159}Cl_2 \cdot 2H_2O$ and $Co_{0.638}Mn_{0.112}Fe_{0.250}Cl_2 \cdot 2H_2O$ also displayed similar characteristics, though in these mixtures slight convex downward

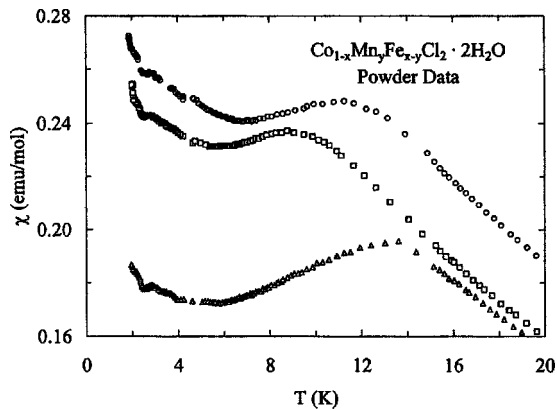FIG. 2. Molar magnetic susceptibility vs temperature below 20 K for three compositions of $Co_{1-x}Mn_yFe_{x-y}Cl_2 \cdot 2H_2O$. Triangles are $1-x = 0.320$, $y = 0.200$; squares are 0.231, 0.423; and circles are 0.101, 0.494, similarly. The latter data are shifted up 0.01 emu/mol for clarity.
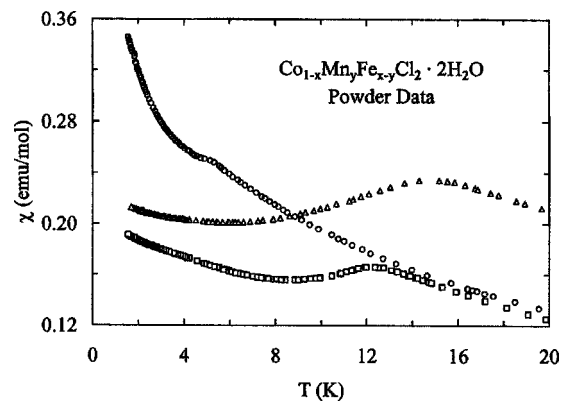

FIG. 3. Molar magnetic susceptibility vs temperature below 20 K for three compositions of $Co_{1-x}Mn_yFe_{x-y}Cl_2 \cdot 2H_2O$. Squares are $1-x = 0.638$, $y = 0.112$; circles are 0.090, 0.810; and triangles are 0.333, 0.067, similarly. The latter are shifted up 0.06 emu/mol for clarity.

TABLE II. $Co_{1-x}Mn_yFe_{x-y}Cl_2 \cdot 2H_2O$ compositions, characteristic temperatures, and irreversibility rank. Values in parentheses are less reliably estimated. The first column under T(anomalies) is a T_c estimate associated with T(max), if it can be made.

$1-x$	y	$x-y$	T(max) (K)	T(anomalies) (K)				Irrev. rank
0.377	0.464	0.159	2.7	2.5	2.1_5			3
0.461	0.377	0.162	(5.5)		2.8	2.4_5		5
0.634	0.272	0.094	10.3	9.2	2.6	2.2	1.8_5	6
0.170	0.681	0.149	2.7	2.4_5	(5.1)	(3.4)		1/2[a]
0.152	0.240	0.608	16.4	13.6	2.7	2.5		9–12
0.320	0.200	0.480	13.6	9.2	3.9	2.9	2.5	9–12
0.101	0.494	0.405	11.2	9.6	2.9	2.5		2/1[a]
0.231	0.423	0.346	8.8	7.5	5.2	2.8	2.5	4
0.638	0.112	0.250	12.3	10.9	3.7			7
0.333	0.067	0.600	14.8	11.3	2.3			9–12
0.090	0.810	0.100	5.1	4.3	(3.1)			9–12
0.535	0.170	0.295	9.6	8.1	1.9			8

[a]Either first or second depending on whether absolute or relative measure of $(M/H)_{FC}-(M/H)_{ZFC}$ is used.

curvature rather than linearity was also apparent in the 4.2 K isotherms. Such was also the case for $Co_{0.170}Mn_{0.681}Fe_{0.149}Cl_2 \cdot 2H_2O$, and though still rather small the hysteresis in the 1.9 K isotherm of this mixture was a bit larger than for the four compositions just mentioned.

Certain compositions contrast qualitatively with those described above. Thus, for $Co_{0.535}Mn_{0.170}Fe_{0.295}Cl_2 \cdot 2H_2O$ in Fig. 5 there is apparent for each of the isotherms a concave upward curvature, rather than convex downward. For the lower temperature isotherm the hysteresis is very noticeable. The isotherms of compositions $Co_{0.320}Mn_{0.200}Fe_{0.480}Cl_2 \cdot 2H_2O$, $Co_{0.461}Mn_{0.377}Fe_{0.162}Cl_2 \cdot 2H_2O$, and $Co_{0.333}Mn_{0.067}Fe_{0.600}Cl_2 \cdot 2H_2O$ also displayed weak concave upward curvature along with only quite small or negligible hysteresis.
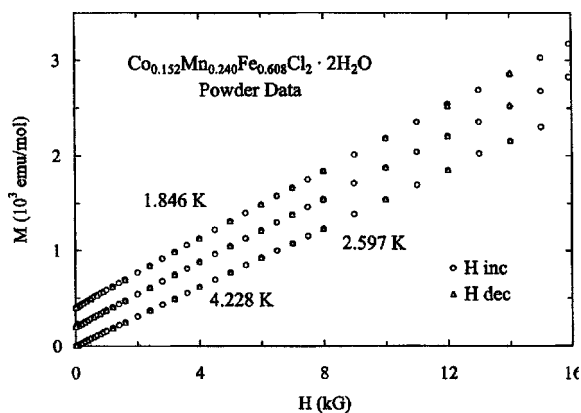
Two compositions displayed isotherms, at any rate for some temperatures, which were distinct in exhibiting an *S* shape, i.e., convex downward curvature at lesser fields and concave upward curvature at larger fields, with an inflection between the two regimes. Thus, in Fig. 6 each isotherm of $Co_{0.101}Mn_{0.494}Fe_{0.405}Cl_2 \cdot 2H_2O$ on close inspection displays an inflection, the location of which (in the 8–12 kG range) appears to increase with decreasing temperature. It is also evident that the hysteresis grows significantly with decreasing temperature. A similar situation occurs for $Co_{0.231}Mn_{0.423}Fe_{0.346}Cl_2 \cdot 2H_2O$.

Finally, one mixture is characterized by certain isotherms with somewhat different behavior from those of the foregoing compositions. For $Co_{0.090}Mn_{0.810}Fe_{0.100}Cl_2 \cdot 2H_2O$ in Fig. 7, while the 4.244 K isotherm may exhibit only modest convex downward curvature, with near negligible hysteresis, the isotherms at 2.404 and 1.852 K are less conventional. More accurate than describing them as also convex downward is to note that while this designation applies to the relatively low
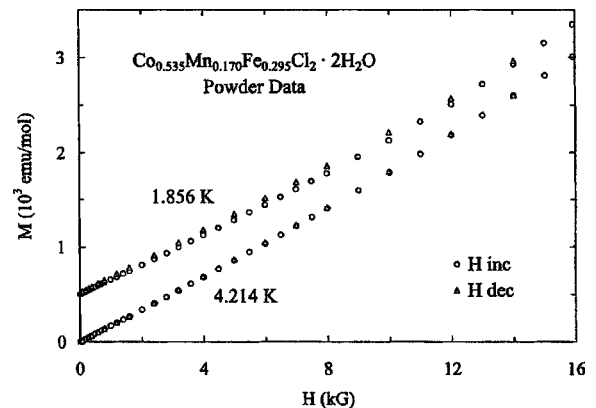

FIG. 4. Molar magnetization vs field for $Co_{0.152}Mn_{0.240}Fe_{0.608}Cl_2 \cdot 2H_2O$ at various temperatures. Temperatures appear up plot in the same order as data sets; for clarity the 2.597 and 1.846 K data are shifted up 200 and 400 emu/mol, respectively.

FIG. 5. Molar magnetization vs field for $Co_{0.535}Mn_{0.170}Fe_{0.295}Cl_2 \cdot 2H_2O$ at two temperatures. For clarity the 1.856 K data are shifted up 500 emu/mol.

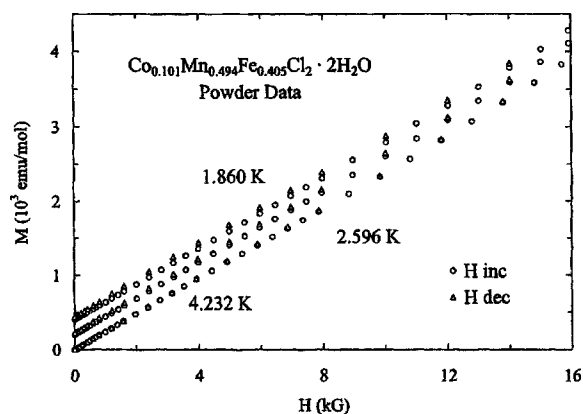FIG. 6. Molar magnetization vs field for $Co_{0.101}Mn_{0.494}Fe_{0.405}Cl_2 \cdot 2H_2O$ at various temperatures. Temperatures appear up plot in the same order as data sets; for clarity the 2.596 and 1.860 K data are shifted up 200 and 400 emu/mol, respectively.

field region, up to a few kG, for fields above about 4 kG there is virtual linearity. Hysteresis is negligible or only very slight.

C. Magnetization irreversibility vs temperature

In Figs. 8–10 appear field-cooled and zero-field-cooled magnetization data (divided by applied field, 200 G in each case) as a function of temperature for three of the twelve compositions. In each case the sample was cooled to a temperature near 1.7 K in zero field, after which a 200 G field was applied, the sample warmed to 4.2 K and then cooled back down in the same field. A substantial variation in degree of irreversibility appears with respect to composition. The mixtures $Co_{0.090}Mn_{0.810}Fe_{0.100}Cl_2 \cdot 2H_2O$, $Co_{0.152}Mn_{0.240}Fe_{0.608}Cl_2 \cdot 2H_2O$, $Co_{0.320}Mn_{0.200}Fe_{0.480}Cl_2 \cdot 2H_2O$, $Co_{0.333}Mn_{0.067}Fe_{0.600}Cl_2 \cdot 2H_2O$, $Co_{0.634}Mn_{0.272}Fe_{0.094}Cl_2 \cdot 2H_2O$ and $Co_{0.638}Mn_{0.112}Fe_{0.250}Cl_2 \cdot 2H_2O$ displayed negligible or at
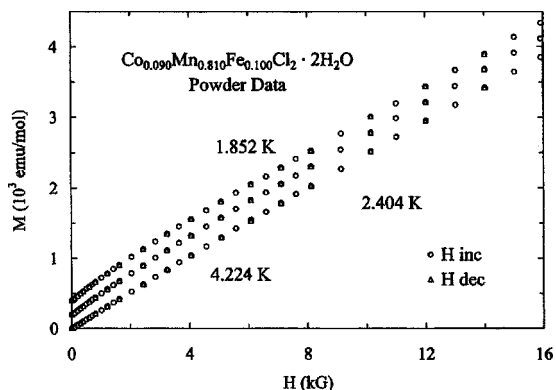
FIG. 7. Molar magnetization vs field for $Co_{0.090}Mn_{0.810}Fe_{0.100}Cl_2 \cdot 2H_2O$ at various temperatures. Temperatures appear up plot in same order as data sets; for clarity the 2.404 and 1.852 K data are shifted up 200 and 400 emu/mol, respectively.
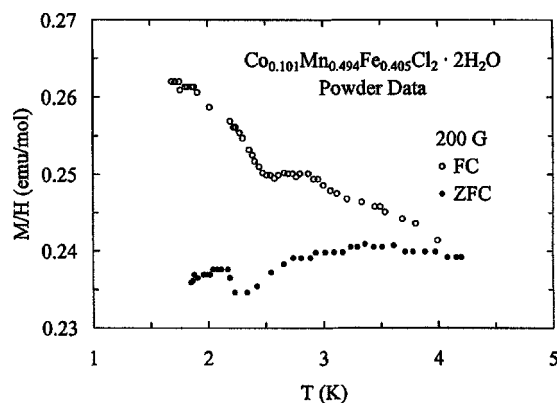

FIG. 8. Temperature dependence of field-cooled and zero-field-cooled magnetizations divided by field for $Co_{0.101}Mn_{0.494}Fe_{0.405}Cl_2 \cdot 2H_2O$.

most only rather small and questionable irreversibility often in some limited temperature range. These are not shown. The data for $Co_{0.461}Mn_{0.377}Fe_{0.162}Cl_2 \cdot 2H_2O$ (also not shown) were rather erratic and suggested a definite irreversibility only below 2.3 K.

Definitely larger or at any rate more unmistakable irreversibilities are displayed by several other compositions. Field-cooled and zero-field-cooled magnetizations for the composition $Co_{0.101}Mn_{0.494}Fe_{0.405}Cl_2 \cdot 2H_2O$ appear in Fig. 8. For $Co_{0.231}Mn_{0.423}Fe_{0.346}Cl_2 \cdot 2H_2O$ the appearance was somewhat similar, with irreversibility existing throughout the temperature range displayed though only about half the size. In both cases features are evident near and above 2.5 K, especially in the field-cooled magnetization. Because the instrumentation does not permit smooth field-warming through 4.2 K, the data for these samples do not have the full significance which an unconstrained field-warming (i.e., to 10 K) and field-cooling set would have.

For the compositions $Co_{0.377}Mn_{0.464}Fe_{0.162}Cl_2 \cdot 2H_2O$ (not shown) and $Co_{0.170}Mn_{0.681}Fe_{0.148}Cl_2 \cdot 2H_2O$ in Fig. 9 inarguable separations between field-cooled and zero-field-cooled data appear at certain temperatures below 4.2 K, and become
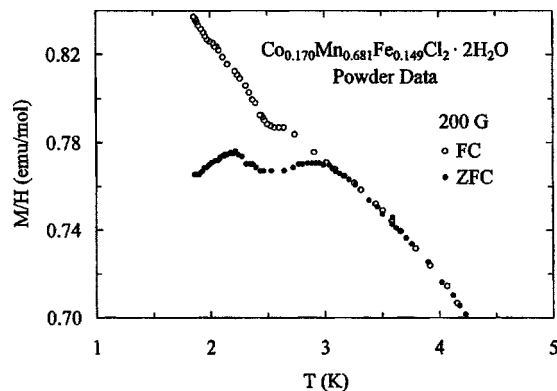

FIG. 9. Temperature dependence of field-cooled and zero-field-cooled magnetizations divided by field for $Co_{0.170}Mn_{0.681}Fe_{0.149}Cl_2 \cdot 2H_2O$.
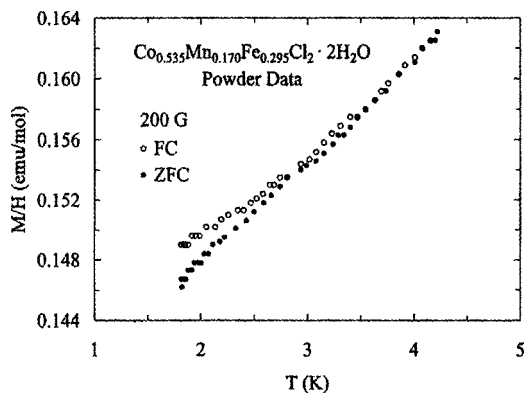
FIG. 10. Temperature dependence of field-cooled and zero-field-cooled magnetizations divided by field for $Co_{0.535}Mn_{0.170}Fe_{0.295}Cl_2 \cdot 2H_2O$.

larger below about 2.5 K, rather as was the case for the mixture of Fig. 8. The Fig. 9 mixture has by far the largest absolute irreversibility near 1.7 of any composition, and is second largest (after the Fig. 8 mixture) on a relative basis, i.e., $\Delta(M/H)/(M/H)_{FC}$.

The behavior for $Co_{0.535}Mn_{0.170}Fe_{0.295}Cl_2 \cdot 2H_2O$ in Fig. 10 is unique in that the magnetization decreases uniformly with decreasing temperature. Also evident is a corresponding gradual increase in the difference between field-cooled and zero-field-cooled data. In Table II the compositions are ranked according to the $(M/H)_{FC} - (M/H)_{ZFC}$ difference at 1.8 K as a measure of irreversibility.

D. Irreversibility line

For one composition, $Co_{0.170}Mn_{0.681}Fe_{0.149}Cl_2 \cdot 2H_2O$, sufficient data of suitable quality could be collected to determine the variation with field of a characteristic irreversibility temperature. This is also the mixture where the magnetization irreversibility was largest. Field-cooled and zero-field cooled magnetization data analogous to those in Fig. 9 were obtained in four other applied fields, of approximately 100 G, 1 kG, 2 kG, and 5 kG. The temperature at which the field-cooled and zero-field-cooled data separate is estimated with reasonable precision (it is 3.00 K for the Fig. 9 data) and was found to decrease monotonically as the field increased.

It appears from the example in Fig. 9 that at some yet lower temperature there develops a larger separation. This might be a transition to "strong" irreversibility, the higher temperature (initial separation) being that for a transition to "weak" irreversibility. However, it did not prove possible to estimate a strong irreversibility onset for most of the five (field) data sets; hence, the existence of such a transition should be considered uncertain in this system. In general, irreversibility lines for spin glasses can be represented by a form

$$\tau_g = ch^a, \quad (1)$$

where the reduced temperature $\tau_g = 1 - T_g(H)/T_g(0)$, where the reduced field $h = \mu H / k T_g(0)$, with the spin magnetic mo-
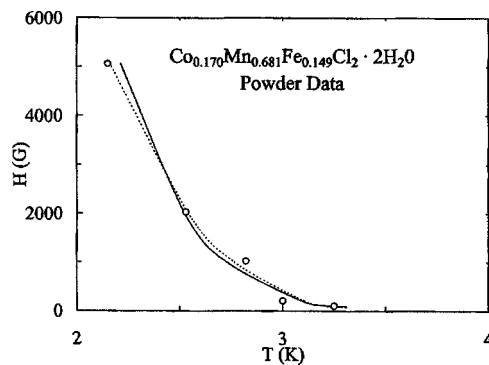

FIG. 11. Weak irreversibility line for $Co_{0.170}Mn_{0.681}Fe_{0.149}Cl_2 \cdot 2H_2O$. The solid curve is an optimal fit, described in text, with $T_g(0) = 4.12$ K; dashed curve is a less than optimal but still good fit with $T_g(0) = 3.60$ K.

ment μ equal to $g\mu_\beta[S(S+1)]^{1/2}$ and where a is a simple fraction or an integer in certain models,[27,28] but may differ from such idealized values in real materials.

In Fig. 11 appears the applied field H and associated weak irreversibility temperature $T_{w(eak)}$ for the five measuring fields. It was found that an optimal fit to the form Eq. (1), but with H instead of h and c' instead of c, occurs for $T_g(0) = 4.12$ K, $a = 0.193$, and $c' = 0.0893_1$. This is represented by the solid curve in the figure. It was also determined that modest shifts in $T_g(0)$ do not worsen the fit very much. In the susceptibility of this sample a subtle but clear anomaly appears near 3.6 K. If one employs a $T_g(0)$ value of 3.60 K, instead of 4.12 K, an only slightly worse fit is obtained with parameters $a = 0.333$ and $c' = 0.0233_8$. This is represented by the dashed curve in Fig. 11, which actually appears visually to be the superior fit.

E. Thermoremanent magnetization (TRM)

This quantity was measured for most of the mixtures listed fifth through twelfth in Tables I and II, though not for the first four. The TRM is obtained by cooling the sample in an applied field from an initial temperature above any pos-
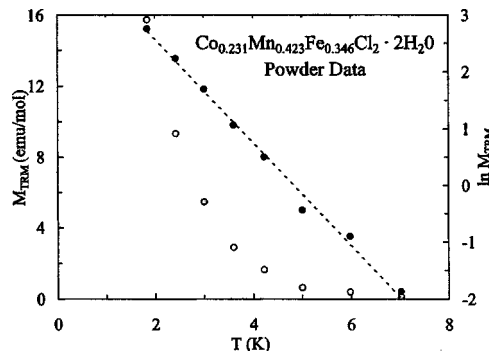
FIG. 12. Thermoremanent magnetization vs temperature for $Co_{0.231}Mn_{0.423}Fe_{0.346}Cl_2 \cdot 2H_2O$, after 1.5 kG field cooling and measured at 300 s. Open and closed circles are with respect to left and right vertical scales, respectively. Dashed line is a linear fit to the ln M_{TRM} vs T representation.

FIG. 13. Thermoremanent magnetization vs temperature for $Co_{0.535}Mn_{0.170}Fe_{0.295}Cl_2 \cdot 2H_2O$, after 1.5 kG field cooling and measured at 300 s. Open and closed circles are with respect to left and right vertical scales, respectively. Dashed line is a linear fit to the ln M_{TRM} vs T representation.
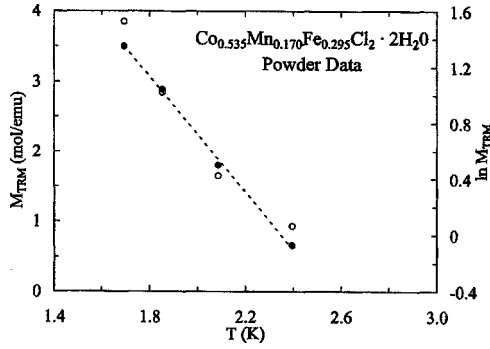
sible spin glass transition (T_g) to some final measuring temperature, decreasing the field to zero, and observing the decaying remanent magnetization. A 1.5 kG cooling field was employed in the present work, and the initial temperature was above 20 K.

1. Temperature dependence

In Figs. 12 and 13 appear the temperature dependences of the TRM for two of four mixtures where a sufficient number of different temperatures were available; in each case, and arbitrarily, the observation made 300 s after turning off the cooling field is employed. For $Co_{0.101}Mn_{0.494}Fe_{0.405}Cl_2 \cdot 2H_2O$ (not shown) and $Co_{0.231}Mn_{0.423}Fe_{0.346}Cl_2 \cdot 2H_2O$ the TRM is large. Interestingly, despite its greater magnitude at the lowest temperatures for the former composition, it also falls faster and is more difficult to observe above 6 K than for the latter. For $Co_{0.535}Mn_{0.170}Fe_{0.295}Cl_2 \cdot 2H_2O$ and $Co_{0.090}Mn_{0.810}Fe_{0.100}Cl_2 \cdot 2H_2O$ (not shown) the TRM is substantially smaller, and also appears to be approaching an essentially nil value at some temperature below 4.2 K. Certain simple forms for the temperature dependence of the TRM have sometimes been observed in spin glass systems. Two common ones are $M_{TRM} \propto \exp(T^*/T)$, with T^* a characteristic temperature (energy) and with this description corresponding to an activation process of some kind, and $M_{TRM} \propto \exp(-\beta T)$. Plots of ln M_{TRM} vs $1/T$ were definitely not linear for the four mixtures mentioned above. However, as

TABLE III. $Co_{1-x}Mn_yFe_{x-y}Cl_2 \cdot 2H_2O$ compositions with thermoremanent magnetization analysis.

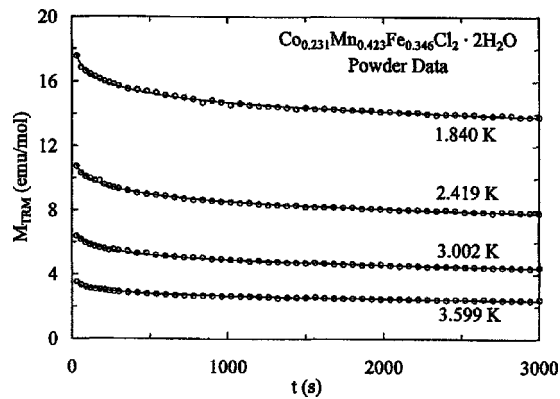| $1-x$	y	$x-y$	$\beta(K^{-1})$	$T'(K)$	$T(K)$	$M_0\left(\dfrac{emu}{mol}\right)$	$S\left(\dfrac{emu}{mol}\right)$	$T_0(K)$	$\tau_0(s)$
0.101	0.494	0.405	1.178	6.0	1.845	44.12	1.864	6.2–6.5	10^{-12}
					2.404	24.72	1.276		
					3.002	16.35	1.230		
					3.598	7.46	0.613		
					4.223	3.07	0.228		
					5.031	1.56	0.116		
					5.985	0.350	0.028		
0.231	0.423	0.346	0.901	7–8	1.840	20.36	0.818	7.5–8.0	10^{-13}
					2.419	13.06	0.655		
					3.002	7.99	0.449		
					3.599	4.26	0.234		
					4.218	2.28	0.106		
					5.066	0.924	0.044		
					5.977	0.516	0.019		
					7.017	0.350	0.028		
0.638	0.112	0.250			1.853	5.55	0.407	2.9–3.5	10^{-12}
					2.102	2.71	0.177		
					2.406	1.69	0.080		
0.090	0.810	0.100	3.508	2.6–3.0	1.694	3.16	0.344	2.5–3.0	
					1.845	1.52	0.150		
					2.002	0.549	0.033		
					2.102	0.392	0.017		
					2.202	0.314	0.011		
0.535	0.170	0.295	2.046	2.8–3.2	1.694	6.32	0.431	2.9–3.5	10^{-12}
					1.852	4.73	0.331		
					2.087	2.81	0.199		
					2.396	1.57	0.111		

FIG. 14. Time dependence of thermoremanent magnetization at temperatures below 4.2 K after 1.5 kG field cooling of $Co_{0.231}Mn_{0.423}Fe_{0.346}Cl_2 \cdot 2H_2O$. Curves are fits according to Eq. (2).

FIG. 16. Temperature dependence of Eq. (2) fit parameters for thermoremanent magnetization decay in $Co_{0.231}Mn_{0.423}Fe_{0.346}Cl_2 \cdot 2H_2O$. Open symbols are M_0; closed are S. Curves through results are guides to the eye only.

the alternative representation in Figs. 12 and 13 reveals, ln M_{TRM} vs T is fairly linear, agreeing with the last form given. The value of β for the four mixtures noted appears in Table III. It is interesting to observe that the order of increase in β is close to the order of decreasing irreversibility, as indicated by the general size of the TRM or the magnitude of the difference $(M/H)_{FC} - (M/H)_{ZFC}$. Also shown in the table is an estimate, T', of the temperature where the TRM reaches zero.

2. Time dependence

In Figs. 14 and 15 appear the time dependences of the TRM at various temperatures for two of the five compositions for which the TRM decay was followed. For the mixture of Fig. 14 the TRM was also followed at several temperatures between 4.2 and 7 K; these data are not shown because the TRM and its decay are too small to be well discerned on the scale of the figure. Instrumental limitations prevent the TRM from being followed for much more than 3000 seconds, and occasionally somewhat less. For applied fields of the magnitude used here we have not found it possible in the past to observe wait-time effects, and such were not explored here. Initial graphical analysis in order to test
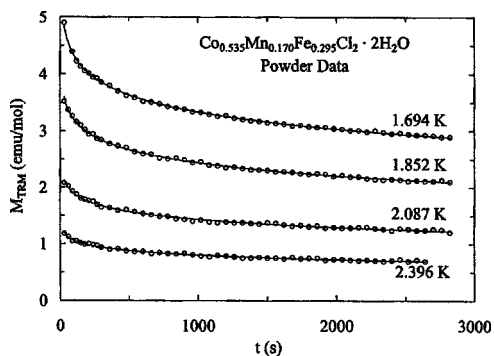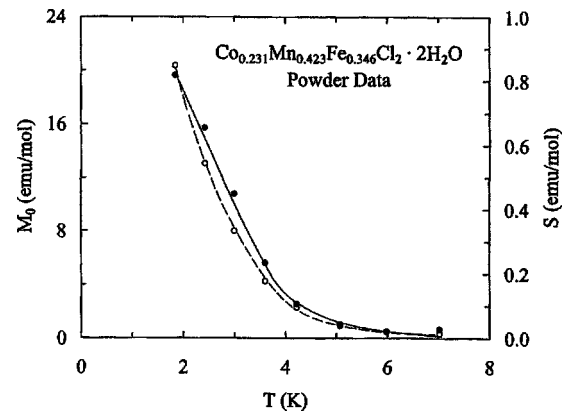
for simple algebraic ($M_{TRM} \propto t^{-a}$) or logarithmic time dependences suggested that, indeed, the latter form,

$$M_{TRM}(t) = M_0 - S \ln t \qquad (2)$$

was likely to be as good or better in reproducing observation than a stretched exponential form which we (and others) have often found worked best in other systems,[29,30]

$$M_{TRM}(t) = M_0 \exp[-(t/\tau)^b]. \qquad (3)$$

Using the latter expression attempts were made both allowing the exponent b to vary and fixing it at a plausible value, based on experience with other spin glass systems, of 0.33.

In each of Figs. 14 and 15 the curves through the data are fits according to the logarithmic form Eq. (2), which generally yielded smaller rms deviations than did the stretched exponential form Eq. (3). Such rms deviations were typically in the range of a few 0.1% to 1.5% for all but the highest temperature data sets, where much larger values followed mainly from the large scatter of the now fairly small TRM data. An exception is $Co_{0.090}Mn_{0.810}Fe_{0.100}Cl_2 \cdot 2H_2O$, where all rms deviations are at least several percent because all the TRM sets are fairly small and the effects of scatter magnified. It might be mentioned that for the two lowest temperature data sets of this sample, a fit according to Eq. (3) was somewhat superior. Given the scatter in the data we do not attach much significance to this. The temperatures of these data sets for the five compositions and the M_0 and S fit parameters appear in Table III.

In Figs. 16 and 17 appear the best fit parameters vs temperature for two of the five compositions according to the Eq. (2) form. Both M_0 and S decrease smoothly with increasing temperature and tend to zero value for some temperature, call it T_0, not too different from the limit of each plot. The estimated ranges for T_0 for each of the five compositions appear in Table III. Sometimes this temperature appears to be slightly higher based on $S(T)$ than on $M_0(T)$, sometimes the reverse. While precise extrapolations cannot be made, it is clear that there are substantial differences among T_0 values for most mixtures.
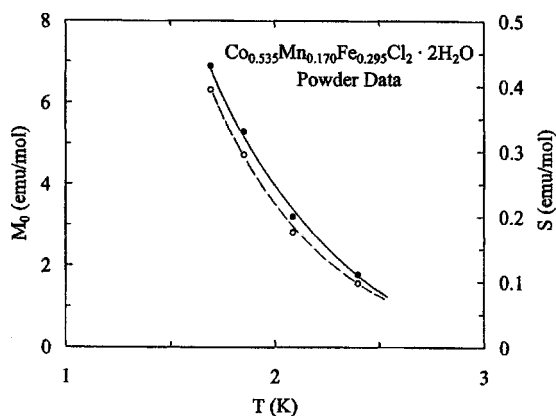

FIG. 15. Time dependence of thermoremanent magnetization at various temperatures after 1.5 kG field cooling of $Co_{0.535}Mn_{0.170}Fe_{0.295}Cl_2 \cdot 2H_2O$. Curves are fits according to Eq. (2).

FIG. 17. Temperature dependence of Eq. (2) fit parameters for thermoremanent magnetization decay in $Co_{0.535}Mn_{0.170}Fe_{0.295}Cl_2 \cdot 2H_2O$. Open symbols are M_0; closed are S. Curves through results are guides to the eye only.

Although the logarithmic decay form worked best, in general, fits according to the stretched exponential form, Eq. (3), were only a bit less good. It is worth noting some trends. In Eq. (3) fits the prefactor M_0, though taking somewhat different numerical values than in Eq. (2) fits, showed the same general temperature dependence. It is interesting to compare τ values, employing in each case the result from fitting the 1.8 K data set, since a common temperature with fairly precise data that were adequately fit. For $Co_{0.090}Mn_{0.810}Fe_{0.100}Cl_2 \cdot 2H_2O$, $Co_{0.638}Mn_{0.112}Fe_{0.250}Cl_2 \cdot 2H_2O$, $Co_{0.535}Mn_{0.170}Fe_{0.295}Cl_2 \cdot 2H_2O$, $Co_{0.101}Mn_{0.494}Fe_{0.405}Cl_2 \cdot 2H_2O$, and $Co_{0.231}Mn_{0.423}Fe_{0.346}Cl_2 \cdot 2H_2O$, these values were 95.4 s, 1197 s, 1692 s, 8.78×10^4 s, and 1.493×10^5 s, respectively. In each of these fits the value of b was allowed to vary, and there is a significant range in the fitted values: $b = 0.182$, 0.154, 0.150, 0.377, and 0.318, respectively.

3. $T \log_{10}(t/\tau_0)$ scaling

The proposal that the TRM in spin glasses scales as $T \log_{10}(t/\tau_0)$, where τ_0 is a microscopic spin flip time, has been confirmed in several such systems.[31,32] It has also been obtained in simulations of both infinite- and short-range spin glass models.[33] Whenever relaxation occurs by thermal activation over barriers for which barrier height does not depend on temperature, this form is expected. The relaxation in small particle systems scales in this fashion also.[34]

In order to test the above, scaling form plots of $\log_{10} M_{TRM}$ vs $T \log_{10} t + pT$ were constructed for each composition with the TRM measured at several different temperatures. Different $p(=-\log_{10} \tau_0)$ were assumed in constructing a series of plots for each composition, and the one with the best overall conformance of the TRM sets to a single curve (scaling function) was judged optimal. Two of these appear in Figs. 18 and 19. Only for $Co_{0.090}Mn_{0.810}Fe_{0.100}Cl_2 \cdot 2H_2O$ (not shown) was it impossible to find any reasonably satisfactory p value to achieve scaling. It is believed that the very small size of the TRM in this case, hence relatively more affected by small systematic
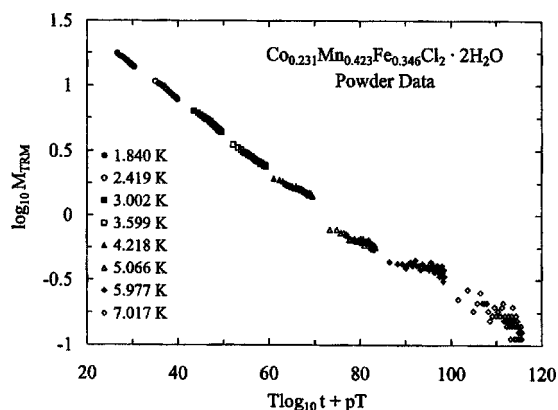

FIG. 18. Optimal $T \log_{10}(t/\tau_0)$ scaling plot for thermoremanent magnetization decay in $Co_{0.231}Mn_{0.423}Fe_{0.346}Cl_2 \cdot 2H_2O$, for $p = 13$.

errors (shifts) among the data sets, is probably responsible for the failure. Scaling is quite satisfactory for $Co_{0.101}Mn_{0.494}Fe_{0.405}Cl_2 \cdot 2H_2O$ (not shown) and for $Co_{0.231}Mn_{0.423}Fe_{0.340}Cl_2 \cdot 2H_2O$. For $Co_{0.535}Mn_{0.170}Fe_{0.295}Cl_2 \cdot 2H_2O$ the scaling is only a bit less satisfactory. For $Co_{0.638}Mn_{0.112}Fe_{0.250}Cl_2 \cdot 2H_2O$ (not shown) scaling is somewhat worse but still plausible. For three of these compositions a p of 12, hence $\tau_0 = 10^{-12}$ s, worked best, and for one $p = 13$, hence $\tau_0 = 10^{-13}$ s. The τ_0 should be considered determined to within one order of magnitude, and appear in Table III.

F. Magnetic phase diagram

Since two independent composition variables exist in a three-component mixture the dependence of magnetic ordering temperature on composition can be fully displayed only in a three-dimensional plot, i.e., $T(x,y)$. We show such in Fig. 20, viewed from what was judged the best perspectives for visualization. (For convenience the more natural compositional variable $1-x$ is employed instead of x.) The depicted surface is generated by connecting most neighboring points in T, x, y space. The resulting set of connected planes, while not the real surface, is useful as visual guide and coheres as a plausibly shaped contour. Evidence that this is indeed so
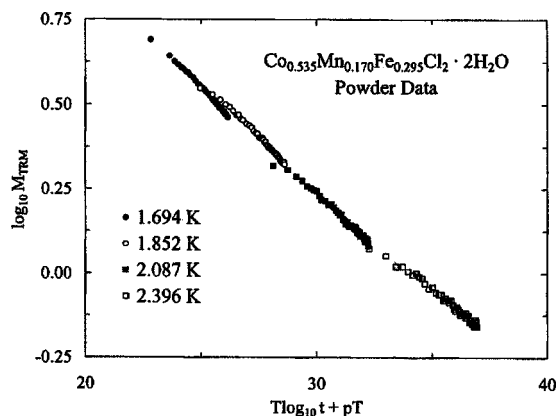

FIG. 19. Optimal $T \log_{10}(t/\tau_0)$ scaling plot for thermoremanent magnetization decay in $Co_{0.535}Mn_{0.170}Fe_{0.295}Cl_2 \cdot 2H_2O$, for $p = 12$.
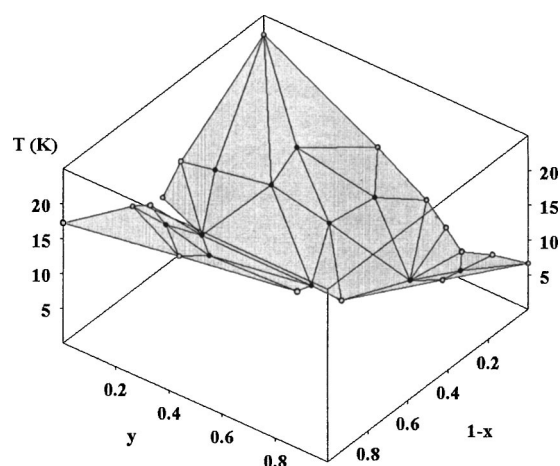
FIG. 20. Magnetic ordering temperature vs composition in $Co_{1-x}Mn_yFe_{x-y}Cl_2 \cdot 2H_2O$. Open circles are taken from the three binary phase diagrams. Contour surface, approximate and primarily a visual guide, is formed by connecting most neighboring points in T, x, y space.

presented itself as the viewing perspective was varied through arbitrary rotations of frame on a computer screen.

Because some T_c estimates are at least a bit uncertain, since inferred from occasionally subtle anomalies in $\chi(T)$, it may be asked whether the $T(x, y)$ diagram would appear different if the more obvious $T(\text{max})$, appearing in most $\chi(T)$, were plotted instead. The general shape of the contour was found to be quite similar to that in Fig. 20, though specific numerical temperature values are of course shifted.

IV. DISCUSSION

The determination of a $T(x, y)$ phase boundary for a ternary magnetic system has not, so far as we know, been reported before. Thus the results in Fig. 20 may be the first of their kind. Known results for the three binary mixtures studied previously are incorporated. However, only the highest temperature transition in any mixture is exhibited. In the ternary mixtures studied here any lower temperature transitions are identified only with significantly more uncertainty. Also, lower temperature transitions and corresponding phase diagram structure for the three binary mixtures are such that attempting to show these as well would make the figure overly complicated. Fairly well-defined behavior is revealed, which may be described as descent to a valley (in temperature) along surfaces originating at limits corresponding to the three binary phase diagrams Fe/Co($y=0$), Fe/Mn($x=1$), and Co/Mn($x=y$).

From Table I it is evident that Curie constants calculated assuming a simple mole fraction weighted average as appropriate are in fair agreement with observed values. The rms percent deviation over the twelve compositions in the table is 3.4%. For the more highly variable θ it is more reasonable to calculate the absolute rms deviation; this is 3.8 K. Most differences between $\theta(\text{obs})$ and $\theta(\text{calc})$ are substantially smaller than this value, yet are still typically several times the general theta uncertainty of 0.4 K. Of course, θ is a multi-ion

interaction based parameter, i.e., in mean field theory[35]

$$\theta = [2S(S+1)/3k]\sum_j z_j J_{ij}, \qquad (4)$$

where the sum is over all interacting neighbors j (z_j such of type j) to a given spin site i, and where the exchange interaction convention is $H_{ex} = -2J_{ij}\underline{S}_i \cdot \underline{S}_j$. Hence, the mole fraction weighted averaging assumption for calculating θ may be quite wrong. The degree of disagreement between observed and calculated thetas supports this judgment. It should be recognized, of course, that in the mixtures there will occur unlike-ion interactions not present in any of the pure components, which presents another reason for not expecting the foregoing calculation of θ to work. It may be mentioned that if one focuses on the cases of largest difference between $C(\text{obs})$ and $C(\text{calc})$, no composition dependent systematics is apparent. The same applies with respect to the largest theta deviations. There is apparent some small overall tendency for $C(\text{calc})$ to be less than $C(\text{obs})$, and for $\theta(\text{calc})$ to be more positive than $\theta(\text{obs})$.

Irreversibility behavior appears in three measured phenomena: magnetization vs field hysteresis, field-cooled vs zero-field-cooled susceptibility (M/H) differences with respect to temperature, and the TRM. The general appearance of magnetization vs field isotherms divides up into three main types as described in Sec. III B: those with convex downward curvature (mainly evident at the lowest temperatures), those with concave upward curvature (similarly), and those showing a change in curvature (S shape) or inflection. The first category exhibited weak to negligible hysteresis at all temperatures. The second kind exhibited small to substantial hysteresis (especially at the lowest temperatures) which depended significantly on composition. The last type showed substantial hysteresis in the two compositions displaying this behavior.

It is difficult to discern compositional systematics which distinguish among the three types of $M(H)$ behavior noted above. The first category especially (convex downward curvature) includes compositions with a wide range of relative Co, Mn, and Fe content. The second category (concave upward curvature) includes only mixtures where the Co content is larger than the Mn, with no apparent restriction on relative Fe content. However, these conditions do not uniquely identify mixtures in this category. The third category (S shape) is represented by two compositions for which each of the Mn and Fe contents substantially exceed the Co, yet for which Fe is not the majority component (Mn being somewhat more prevalent). These conditions are exclusive to this category. As noted in Sec. III B, the mixture $Co_{0.090}Mn_{0.810}Fe_{0.100}Cl_2 \cdot 2H_2O$ exhibits behavior which is arguably distinct from the above types (though still convex downward for small fields). Here one component (Mn) is greatly more prevalent than the other two. Arguably, however, $Co_{0.170}Mn_{0.681}Fe_{0.149}Cl_2 \cdot 2H_2O$ (first category above) also fits this description.

A standard measure of magnetic irreversibility is the difference between field-cooled and zero-field-cooled magnetizations, as surveyed in Sec. III C and displayed in the figures. The one clear compositional systematic which emerges

is that the irreversibility is promoted by a majority combined Co plus Mn content with the Mn at least somewhat more prevalent than the Co. These conditions characterize the first through fourth most irreversible mixtures as ranked in Table II. The compositions ranked fifth through eighth have majority Co plus Mn content, but also Co more prevalent than Mn. The least irreversible mixtures, ranked 9–12 in the table, have either minority Co plus Mn content, barely above majority Co plus Mn content (with Co more prevalent than Mn), or evince a somewhat unique composition. This last refers to $Co_{0.090}Mn_{0.810}Fe_{0.100}Cl_2 \cdot 2H_2O$ where the predominance of one component is most extreme; this excessive dominance appears to be more significant than the criteria of Co and Mn content already remarked. The result here seems consistent with the finding in our work on $Co_{1-x}Mn_xCl_2 \cdot 2H_2O$ that near the composition extremes of this binary system irreversibilities were decidedly weaker.[12] The substitution of some Fe for some Co does not alter that conclusion. Perhaps surprisingly, the degree of hysteresis in magnetization vs field isotherms discussed earlier correlates only rather imperfectly with the irreversibility rankings just reviewed, based on field-cooled vs zero-field-cooled differences.

The TRM results, though not obtained for all mixtures, are quite consistent with the foregoing irreversibility rankings. Thus $Co_{0.101}Mn_{0.494}Fe_{0.405}Cl_2 \cdot 2H_2O$ shows the largest TRM at various temperatures and is one of the two most irreversible compositions in Table II. Among mixtures studied in detail, $Co_{0.231}Mn_{0.423}Fe_{0.346}Cl_2 \cdot 2H_2O$ has the next largest TRM and ranks fourth in Table II. A substantially smaller TRM is displayed by $Co_{0.638}Mn_{0.112}Fe_{0.0250}Cl_2 \cdot 2H_2O$, which ranks seventh in Table II. A yet slightly smaller TRM is found for $Co_{0.535}Mn_{0.170}Fe_{0.295}Cl_2 \cdot 2H_2O$, which ranks eighth. A much smaller TRM is observed for $Co_{0.090}Mn_{0.810}Fe_{0.100}Cl_2 \cdot 2H_2O$, ranked ninth through twelfth. Three other compositions, listed in Table II and also ranked ninth through twelfth, had comparable size TRMs which were not studied (and are not shown) in similar detail.

Somewhat unexpected, because not clearly observed in our previous studies of other mixed magnetic insulating systems with spin glass phases,[12,30,32] is the temperature dependence of the TRM found here: $M_{TRM} \propto \exp(-\beta T)$. This form has been obtained theoretically, albeit in the case of metallic alloy spin glasses in which RKKY interactions and dipolar interactions operate.[36] It has, however, also been observed in the insulating spin glasses $Eu_{0.4}Sr_{0.6}S$ and $ZnCr_{1.6}Ga_{0.4}O_4$.[37,38]

It consistently emerged, as noted in Sec. III E 2, that a logarithmic form for the TRM decay, Eq. (2), gave better fits than did a stretched exponential. A simple power law (algebraic) worked distinctly less well. This was a bit surprising because it is in contrast to our findings in other mixed magnetic insulators showing spin glass phases, including the related system $Co_{1-x}Mn_xCl_2 \cdot 2H_2O$, where fits according to Eq. (3) proved best.[12] However, in our study of $Fe_{1-x}Mn_xCl_2 \cdot 2H_2O$, also related to the present ternary system, logarithmic time dependences were observed.[8] While less commonly seen than the stretched exponential form, logarithmic decays have been reported in a variety of spin glasses, both metallic and insulating. Such decay had also

been predicted early on in the field of rock magnetism, based on thermal activation of particle magnetizations over energy barriers.[39] It has also been noted that the time frame of observation can influence what is seen, and that a logarithmic form emerges from more complicated forms under typical experimental conditions.[40]

The temperature dependence of the fit parameters M_0 and S in Eq. (2) yielded, as in Figs. 16 and 17, what appear to be fairly reliable estimates for the T_0 (ranges) where these parameters fall to zero, which might be expected to have physical significance. These estimates agree fairly well with the somewhat analogous values of T' estimated more directly from TRM(T). From Tables II and III, they are obviously much different (except for $Co_{0.231}Mn_{0.423}Fe_{0.346}Cl_2 \cdot 2H_2O$) from $T(max)$ or estimated T_c values. Nor does there appear any consistent association with (certain of) the lower temperature anomalies listed in Table II. Typically, the T_0 are somewhat higher than the temperatures where differences in $(M/H)_{FC}$ and $(M/H)_{ZFC}$ become clearly evident. This would appear to be the most natural correlation, since detectable irreversibility is the issue by either measure.

For the stretched exponential fits at 1.8 K, it was found that τ displayed a substantial range of variation, from a smallest value of 95.4 s for $Co_{0.090}Mn_{0.810}Fe_{0.100}Cl_2 \cdot 2H_2O$ to a largest value of 1.493×10^5 s for $Co_{0.231}Mn_{0.423}Fe_{0.346}Cl_2 \cdot 2H_2O$. Although imperfect, there is a trend of larger τ, that is slower decay, for mixtures of greater irreversibility. In the preferred logarithmic fits the parameter S, sometimes called the magnetic viscosity coefficient, displays a tendency to increase as the irreversibility increases according to the ranking in Table II. Both of these tendencies are physically reasonable.

The τ_0 deduced from suitable scaling of the TRM in Sec. III E 3, 10^{-12} to 10^{-13} s, are very much in the range typically found for spin glasses, 10^{-11} to 10^{-14} s. For each of $Co_{0.101}Mn_{0.494}Fe_{0.405}Cl_2 \cdot 2H_2O$ and $Co_{0.231}Mn_{0.423}Fe_{0.346}Cl_2 \cdot 2H_2O$, it appears that the scaling begins to fail at some temperature not far above 4.2 K. Such correspond to approximately 55–70% of the T_0 values for these mixtures, which might be taken as plausible approximations to spin glass transition temperatures. In fact, the scaling invoked here is expected to fail for temperatures above about $2T_g/3$, due to departure of barrier height distribution from T independence as $T \rightarrow T_g^-$.[31] For $Co_{0.535}Mn_{0.170}Fe_{0.295}Cl_2 \cdot 2H_2O$ apart from some irregularity regarding the two lowest temperatures, the scaling holds through the highest measured temperature of 2.396 K, which is somewhat less than the T_0 estimated for this mixture. A similar T range of validity as referred to above is at any rate possible. For $Co_{0.638}Mn_{0.112}Fe_{0.250}Cl_2 \cdot 2H_2O$, not shown, the success of the scaling is less clear, but it is plausible that a breakdown occurs between 2.1 and 2.4 K, which is consistent with the cited validity range.

For $Co_{0.170}Mn_{0.681}Fe_{0.149}Cl_2 \cdot 2H_2O$ it proved possible to determine a weak irreversibility line $T(H)$. The coefficients c' reported in Sec. III D, based on using the actual applied fields in the analysis, can be transformed into the more theoretically relevant c of Eq. (1). The relation $C = N_o\mu^2/3k$, where (capital) C is the observed Curie constant, is em-

ployed in order to obtain the effective magnetic moment for this particular mixture. Then the definition $h = \mu H / k T_g(0)$ is used in order to relate h to H. Two possible fits were reported earlier, one with $T_g(0) = 4.12$ K and one with $T_g(0) = 3.60$ K. From the foregoing information the resulting values of c in Eq. (1) are 0.535 in the first case, and 0.490 in the second, associated with the same exponent values already provided, $a = 0.193$ and 0.333, respectively.

A review of the main predictions of mean-field theory concerning spin glass irreversibility lines—including the effects of anisotropy but obtained in the context of infinite range interactions—is given in Ref. 30. A number of scenarios arise, in most of which the exponent a in Eq. (1) takes values substantially larger than those obtained in the present fits; e.g., $a = 2/3$ for the de Almeida–Thouless (AT) line in an Ising spin glass,[27] and $a = 2$ for the Gabay-Toulouse (GT) line in an isotropic m-component spin glass.[28] Anisotropy leads to various cases distinguished by its strength relative to exchange interactions. One intermediate case (where the anisotropy is neither very strong nor merely somewhat less than that, but is one stage stronger than for a so-called weak anisotropy regime) may be relevant here, because the predicted exponent is $a = 1/3$ and both transverse and longitudinal irreversibilities occur together.[41,42] Any estimate of the relative average anisotropy and exchange strengths in $Co_{0.170}Mn_{0.681}Fe_{0.149}Cl_2 \cdot 2H_2O$ is necessarily very approximate, even speculative. But plausible numerical values are consistent with the validity range for the prediction just cited. At any rate this regime seems more likely than the two theoretical regimes of stronger relative anisotropy, where the predicted exponent is quite different. A theoretical prediction for the prefactor is not available in this case. Known prefactors for the more standard scenarios tend to be somewhat less than unity. Hence, on general grounds, the values obtained in the present fits, near $c = 0.5$, seem plausible.

Mention will also be made of the relatively more recent result for the irreversibility line of a short-range Ising spin glass, $\tau_g \propto h^{0.53}$.[43] The exponent here is less than in most infinite range scenarios, but certainly higher than we observe. The prefactor is not available in this case either.

ACKNOWLEDGMENTS

[1] B. Morosin and E. J. Graeber, Acta Crystallogr. **16**, 1176 (1963).

[2] B. Morosin and E. J. Graeber, J. Chem. Phys. **42**, 898 (1965).

[3] K. Katsumata, M. Kobayashi, T. Sato, and Y. Miyako, Phys. Rev. B **19**, 2700 (1979).

[4] M. Kobayashi, K. Katsumata, T. Sato, and Y. Miyako, J. Phys. Soc. Jpn. **46**, 1467 (1979).

[5] K. Katsumata, M. Kobayashi, and H. Yoshizawa, Phys. Rev. Lett. **43**, 960 (1979).

[6] K. Zenmyo and H. Kubo, J. Phys. Soc. Jpn. **66**, 1495 (1997).

[7] S. Fishman and A. Aharony, Phys. Rev. B **18**, 3507 (1978).

[8] G. C. DeFotis, C. Pohl, S. A. Pugh, and E. Sinn, J. Chem. Phys. **80**, 2079 (1984).

[9] K. Zenmyo, H. Kubo, H. Deguchi, K. Konishi, and K. Takeda, J. Phys. Soc. Jpn. **69**, 3980 (2000).

[10] K. Zenmyo, H. Kubo, H. Deguchi, and K. Takeda, J. Phys. Soc. Jpn. **71**, 1740 (2002).

[11] S. Fishman and A. Aharony, Phys. Rev. B **19**, 3776 (1979); **21**, 280 (1980).

[12] G. C. DeFotis, D. S. Mantus, E. M. McGhee, K. R. Echols, and R. S. Wiese, Phys. Rev. B **38**, 11486 (1988).

[13] G. C. DeFotis and E. D. Remy, J. Phys. (Paris), Colloq. **49**, C8-1053 (1988).

[14] G. C. DeFotis and K. D. Dell, Phys. Rev. B **50**, 9937 (1994).

[15] H. Deguchi, K. Takahashi, H. Kubo, and K. Takeda, J. Phys. Soc. Jpn. **59**, 1071 (1990).

[16] K. Zenmyo and H. Kubo, J. Phys. Soc. Jpn. **61**, 1025 (1992); **62**, 1025 (1993); **64**, 1320 (1995).

[17] H. Kubo and K. Zenmyo, J. Phys.: Condens. Matter **5**, 3453 (1993).

[18] H. Kubo, K. Zenmyo, and T. Kato, J. Phys. Soc. Jpn. **65**, 4045 (1996).

[19] A. K. Majumdar and P. v. Blankenhagen, Phys. Rev. B **29**, 4079 (1984).

[20] J. Hesse, Hyperfine Interact. **47**, 357 (1989).

[21] Y. Tsuchiya, T. Bitoh, S. Murayama, S. Chikazawa, and Y. Hamaguchi, J. Phys. Soc. Jpn. **65**, 3289 (1996).

[22] A. Bohorquez, L. E. Zamora, and G. A. Perez Alcazar, Phys. Rev. B **49**, 16035 (1994).

[23] S. I. Ohkoshi, Y. Abe, A. Fujishima, and K. Hashimoto, Phys. Rev. Lett. **82**, 1285 (1999).

[24] S. I. Ohkoshi and K. Hashimoto, Phys. Rev. B **60**, 12820 (1999).

[25] G. C. DeFotis, A. C. Beveridge, M. J. Wilkens, Z. J. Fuller, J. G. McMahon, and C. D. Wallo, J. Appl. Phys. **87**, 6540 (2000).

[26] G. C. DeFotis, C. D. Wallo, R. L. Smith, D. B. Bodkin, G. L. Mirabilio, T. R. Leftwich, and A. D. Slansky, J. Magn. Magn. Mater. **272–276**, 1393 (2004).

[27] J. R. L. De Almeida and D. J. Thouless, J. Phys. A **11**, 983 (1978).

[28] M. Gabay and G. Toulouse, Phys. Rev. Lett. **47**, 201 (1981).

[29] R. V. Chamberlin, G. Mozurkewich, and R. Orbach, Phys. Rev. Lett. **52**, 867 (1984).

[30] G. C. DeFotis, G. A. Coffey, C. C. Cinquina, S. Chandarlapaty, W. W. Brubaker, D. J. Krovich, R. V. Chamberlain, and W. R. A. Jarvis, Phys. Rev. B **51**, 15113 (1995).

[31] R. Omari, J. J. Prejean, and J. Souletie, J. Phys. (Paris) **45**, 1809 (1984).

[32] G. C. DeFotis, G. S. Coker, J. W. Jones, C. S. Branch, H. A. King, J. S. Bergman, S. Lee, and J. R. Goodey, Phys. Rev. B **58**, 12178 (1998).

[33] G. Parisi and F. Ritort, J. Phys. I **3**, 969 (1993).

[34] A. Labarta, O. Iglesias, L. Balcells, and F. Badia, Phys. Rev. B **48**, 10240 (1993).

[35] J. S. Smart, *Effective Field Theories of Magnetism* (W. B. Saunders, Philadelphia, 1966), p. 64.

[36] J. L. Tholence and R. Tournier, Physica A **86–88**, 873 (1977).

[37] H. Maletta and W. Felsch, Phys. Rev. B **20**, 1245 (1979).

[38] D. Fiorani, S. Viticoli, J. L. Dormann, J. L. Tholence, and A. P. Murani, Phys. Rev. B **30**, 2776 (1984).

[39] P. Gaunt, Philos. Mag. **34**, 775 (1976).

[40] A. Khater, J. Ferre, and P. Meyer, J. Phys. C **20**, 1857 (1987).

[41] G. Kotliar and H. Sompolinsky, Phys. Rev. Lett. **53**, 1751 (1984).

[42] K. H. Fischer, Z. Phys. B: Condens. Matter **60**, 151 (1985).

[43] F. Ritort, Phys. Rev. B **50**, 6844 (1994).